TABLE III. Stress–particle-velocity Hugoniot points.

Shot number	Stress (kbar)	Particle velocity (mm/μsec)
312–313	1.024	0.0305
314–315	2.629	0.0755
2113	5.455	0.1487
2116	5.484	0.1502
316–317	5.666	0.1544
2107*R*2	7.853	0.2100
2107*R*1	8.248	0.2220
2106	8.361	0.2250
2108	10.984	0.2960
318–319	11.988	0.3200
320–321	18.340	0.4690

unloading in the longitudinal direction (but before lateral relaxation) is to be expected only if the plastic strains during loading and unloading produce little or no zero-pressure volume increase. While this is true of metals, it does not follow that it is true of PMMA. In fact, one can easily visualize a model in which the plastic deformation produces considerable breaking of chain bonds. If such a process is irreversible on the microsecond time scale of these experiments, the broken bonds will represent a net loss in cohesion of the material, and a resulting gain in volume might be expected.

The curve of Fig. 9 labeled "Hugoniot" is drawn through the peak stress–strain points of the individual shots of Table II. A better name might be the "equilibrium" curve, since those stress–strain points on the curve are not attainable through a single, sharp discontinuity in stress from the initial condition and since the material appears to be in a quasistatic equilibrium state. However, an apparent equilibrium on the microsecond time scale of these experiments does not necessarily coincide with equilibrium behavior on a vastly different time scale, such as seconds or years. Therefore, "Hugoniot" is used in the sense that it is the locus of the peak stress–strain states achievable on the microsecond time scale through impact loading of the material.

There is a cusp in the Hugoniot at about 7–8 kbar, which is further evidence of the onset of plastic yielding. The data from the ramp-wave shot No.327 coincide with the Hugoniot up to the cusp as would be expected because that region is nearly elastic. Above the Hugoniot elastic limit the ramp-wave data fall between the Hugoniot and the shock-input stress–strain path of shots 318 and 319. The endpoint of the ramp-wave shot again coincides with the Hugoniot, however. Again, this is consistent with a rate-dependent yield effect, since the strain rate in the ramp-wave shot above the Hugoniot elastic limit is intermediate between the essentially zero strain rates prevailing at the Hugoniot points and the higher strain rates on the loading path of shots 318–319.

In using a calibrated material, it is often convenient to have the Hugoniot points on the stress–particle velocity plane. Table III contains this information.

Fused Silica

The basic characteristics of compressive wave shapes in fused silica, including the ramp-wave front up to about 40 kbar, were first reported by Wackerle in 1962.[31] His wire reflection experimental technique was severely lacking in precision below the 100-kbar stress level when compared to techniques presently available, and he made no observations of rarefaction waves. Nevertheless, he was able to conclude that the fused silica behaved as a nonlinear elastic solid up to the phase change which he measured at 98 kbar. Our present study of fused silica[32] greatly refines Wackerle's compressive wave data in the low-stress region and confirms his assertion of elasticity by determining that the release stress–strain path followed in a rarefaction wave coincides with the compressive stress–strain path which determines the compressive wave shape.

The vitreous SiO_2 samples used in the experiments for this study were made from GE type 151 fused silica. Its density was measured at 2.201 ± 0.001 g/cm^3, and according to the manufacturer, it had an impurity level of about 55 ppm. The velocity of the toe of the ramp-wave front, which should coincide with the dilatational sound velocity, was 5.93 ± 0.01 mm/μsec. Fraser[33] measured the densities and dilatational velocities of a number of vitreous silicas. He found that the dilatational velocity varied up to 0.6% and the density varied up to 0.1%, depending on the fictive temperature[33] of the particular silica. Although Fraser did not study GE type 151 fused silica, one can infer from a comparison of densities and dilatational velocities that the fictive temperature of our samples was probably low, i.e., 900°–1000°C. As previously stated, the material was used as received from the supplier with surfaces from 0 to 500 nm convex and polished to a surface quality of 60–40 [34] or better. Visual inspection of the material showed it to be free of voids and internal strains. All of the experiments were conducted at $22°\pm3°$C.

The nine shots which provided data on the wave propagation characteristics of fused silica are summarized in Table IV. Compressive wave shapes were measured on all but shot 362, which was specifically a rarefaction-wave experiment. Rarefaction wave shapes were measured on shots 351, 363, 354, 355, and 362. The rarefaction data were lost on shots 350 and 353 and were masked by the prior arrival of edge effects (as anticipated) on shots 356 and 357. As can be seen from Table IV, two shots were fired at each of four different experimental conditions, in addition to the rarefaction-wave shot 362. The duplication of experiments again

TABLE IV. Summary of fused-silica stress-wave-measurement experiments.

Shot number	Impact velocity (mm/μsec)	Projectile thickness (mm)	Specimen thickness[a] (mm)	Maximum particle velocity[b] (mm/μsec)	Peak stress (kbar)
350	0.3077	6.457	6.464	0.1538	18.90
351	0.3068	6.485	6.452	0.1534	18.85
353	0.6583	6.454	6.466	0.3291	38.64
363	0.630	6.480	6.485	0.315	37.08
354	0.6262	3.254[c]	6.492	0.5644	65.17
355	0.6326	3.178[c]	6.495	0.5710	65.94
356	0.6160	6.375	25.428	0.3080	36.30
357	0.6182	6.472	25.437	0.3091	36.42
362	0.6138	6.487	0.0	0.3069	36.00

[a] From impact surface to the internal mirror.
[b] At the impact surface.
[c] Projectile plate was a tungsten carbide disk.

demonstrates the repeatability of the material and the instrumentation.

Although the maximum particle velocity at the impact surface varied from 0.15 to 0.57 mm/μsec and the compressive-wave propagation distance varied from 6.5 to 25 mm, it was found that the initial ramp on the compressive wave was always the same simple centered wave. Thus, the ramps for all eight shots superimpose on each other when plotted as u vs t/S, where S is the sample thickness and t is the time after impact. This result is shown in Fig. 10, where the measured u-vs-t profiles are all scaled to an S of 1 cm. The spread in the ramp data of all of the experiments was less than ±4 nsec at any given u when scaled to the 1-cm sample thickness. The data from shots 356 and 357 scaled to 1 cm agreed within ±2 nsec, as might be expected because of the finer resolution provided by the greater sample thicknesses. Data points from Wackerle's[31] "average" compressive wave profile are also shown in Fig. 10. Although Wackerle's data differ from ours by as much as 75 nsec at a given particle velocity, the difference is nevertheless probably within Wackerle's experimental error.

The measured wave profiles indicate a discontinuity in acceleration at the leading edge of the ramps. Thus, the fused-silica wavefront provides an example of a true acceleration wave in nature. The properties of such waves have been explored from a continuum mechanics point of view by several theorists. In particular, Chen[35] cites some of the present data in his review article on acceleration wave phenomena.

Because the wave profiles can be scaled, a single loading stress–strain path will reproduce all of the measured wave profiles, given the appropriate boundary conditions of the individual shots. Points on the stress–strain path were determined by the method described in the section on PMMA, and these points were fit by the fourth-order stress–strain equation

$$\sigma = 776.0\epsilon - 4159\epsilon^2 + 30340\epsilon^3 - 69260\epsilon^4, \qquad (3)$$

where σ is the stress in kilobars. This equation not only fits the present data very well to 65 kbar but also converges to within 1%–2% of Wackerle's[31] data in the 90–95-kbar range. Since Wackerle reported a phase transition in fused silica at 98 kbar, it appears that Eq. (3) may be reasonably good over the entire region up to the phase transition.

The measured rarefaction waves were always originated by the reflection of compressive waves from the rear surface of the projectile nose plate. The rarefaction wave shapes measured on shots 351 and 363 were shocks with rise times (or fall times, if you prefer) too small to be resolved, i.e., less than about 1 nsec. The rarefaction shock in fused silica was also observed by Kusubov[36] with a manganin gauge stress transducer.

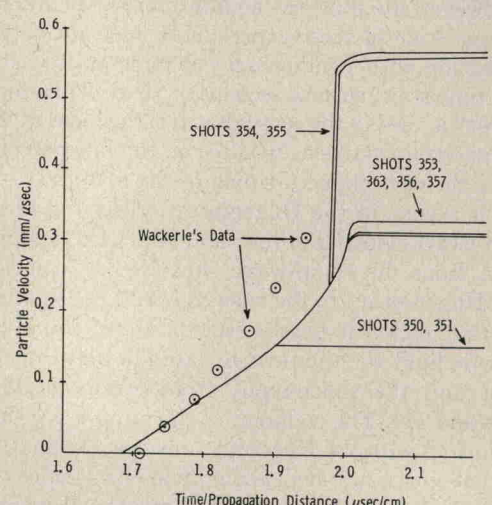

FIG. 10. Compressive wave profiles in fused silica.